Mineralium Deposita (2000) 35: 48–62

ARTICLE

N. R. Herdianita · P. R. L. Browne · K. A. Rodgers
K. A. Campbell

Mineralogical and textural changes accompanying ageing of silica sinter

Received: 18 November 1998 / Accepted: 6 July 1999

Abstract Twenty nine samples of silica sinter, ranging in age from modern to Miocene, record temporal changes in both mineralogy and texture. When first deposited, sinters consist largely of noncrystalline spheres (<1–8 μm diameter) of opal-A exhibiting varying degrees of close-packing. Particle densities range from 1.5 to 2.1 g cm^{-3}, total water 4–10 wt%, and porosities 35–60%. Changes over ~10,000 years following deposition are slight although the spheres may be invested by an additional film of secondary silica. For the next 10,000 to ~50,000 years, the silica incrementally crystallises to become poorly crystalline opal-CT and/or opal-C; spherical particles of thin-bladed crystals (lepispheres) replace opal-A particles and coalesce in microbotryoidal aggregates (~10–30 μm diameter). Amygdaloidal fibrous clusters occur with lepispheres. As silica lattice ordering becomes enhanced, total water content drops to <7 wt%, particle density increases to ~2.3 g cm^{-3}, and porosity reduces to <30%. The change from opal-A to opal-C takes place over a briefer periods (~50 years) in silica sinters that contain other materials (e.g. calcite, sulfur, alunite, plant remains). Sinters older than ~50,000 years have recrystallised to microcrystalline quartz. With the onset of quartz crystallisation at ~20,000 years, total water is <0.2 wt%, particle density approximates quartz (2.65 g cm^{-3}), and porosity is <4%. The progressive changes in silica species and texture yield ageing profiles for sinters that may serve as guides to the paleohydrology of geothermal systems and/or epithermal ore deposits in areas where surface thermal activity has declined or ceased.

Editorial handling: P. Lattanzi

N.R. Herdianita · P.R.L. Browne · K.A. Rodgers (✉) ·
Kathleen A. Campbell
Department of Geology, University of Auckland,
Private Bag 92019, Auckland, New Zealand
e-mail: ka.rodgers@auckland.ac.nz
Fax: +649-3737435

N.R. Herdianita
Department of Geology, Institute of Technology Bandung,
Jalan Ganesa 10 Bandung 40132, Indonesia

P.R.L.Browne
Geothermal Institute, University of Auckland,
Private Bag 92019, Auckland, New Zealand

Introduction

Surface deposits of silica sinter are a common expression of geothermal systems. They are a persistent signature of the hydrological conditions prevailing at the time that the sinter formed and are an important exploration guide to locating and interpreting geothermal systems whose surface activity has changed, declined or even ceased. Deposits of silica sinter are also commonly associated with epithermal ore deposits with a wide range of ages; for example Lihir, Papua New Guinea (still active), McLaughlin, California (Plio-Pleistocene; Sherlock et al. 1995), Hasbrouck, Nevada (Miocene; Graney 1987), Drummond Basin, Queensland (Carboniferous; Cuneen and Sillitoe 1989; White et al. 1989), and Rhynie, Scotland (Devonian; Trewin 1994). In all cases identifying the silica sinter correctly is important in so far as its presence implies that subsurface temperatures were in excess of 175 °C (Fournier and Rowe 1966). In addition, silica sinter forms at the ground surface, usually from alkali chloride waters of near-neutral pH.

One problem in prospecting epithermal ore deposits is distinguishing between true silica sinter and silica residue. The latter consists of silica derived entirely from the destruction of host rocks by acid waters formed from the oxidation of H_2S ascending with steam that then condenses. Steam does not carry metals except mercury, in contrast to alkali chloride waters, and, in hydrologically simple situations, precious metals cannot be expected to be associated with deposits of silica residue. Misidentification of silica sinter can therefore lead to an incorrect interpretation of the palaeohydrology of an epithermal ore deposit or a thermal field.

When first deposited, silica in sinter is characteristically noncrystalline opal-A. However, sinters several hundred years old contain considerable amounts of paracrystalline opal-CT and/or opal-C, whereas microcrystalline quartz is common in sinters older than ~20,000 years (e.g. White et al. 1988). Similar variations in silica species have been reported from microscopic opals in marine sediments and have been ascribed to transformations in silica crystal chemistry during burial diagenesis (e.g. Murata and Nakata 1974; Kano 1983). In the case of sinters, differences in silica species occur in terrestrial rocks that have not necessarily undergone burial and point to a progressive change in sinter mineralogy with time. The present study reports the mineralogical and physical changes found in a series of silica sinter samples of different ages collected from the surface and near surface of several geothermal fields within the long-lived (>1.5 Ma) Taupo Volcanic Zone (TVZ) of New Zealand (Fig. 1). Some Cenozoic sinters from elsewhere are included for comparison. The changes prove to be reasonably systematic, such that the mineralogical state and texture of a sinter can give an indication of its relative age, all other factors being equal.

Nomenclature of the noncrystalline, paracrystalline and microcrystalline silica species follows that of Smith (1997, 1998) (but see Jones and Segnit 1971; Flörke et al. 1991; Graetsch 1994). Textural descriptions follow those of Trewin (1994), Cady and Farmer (1996) and Walter et al. (1996).

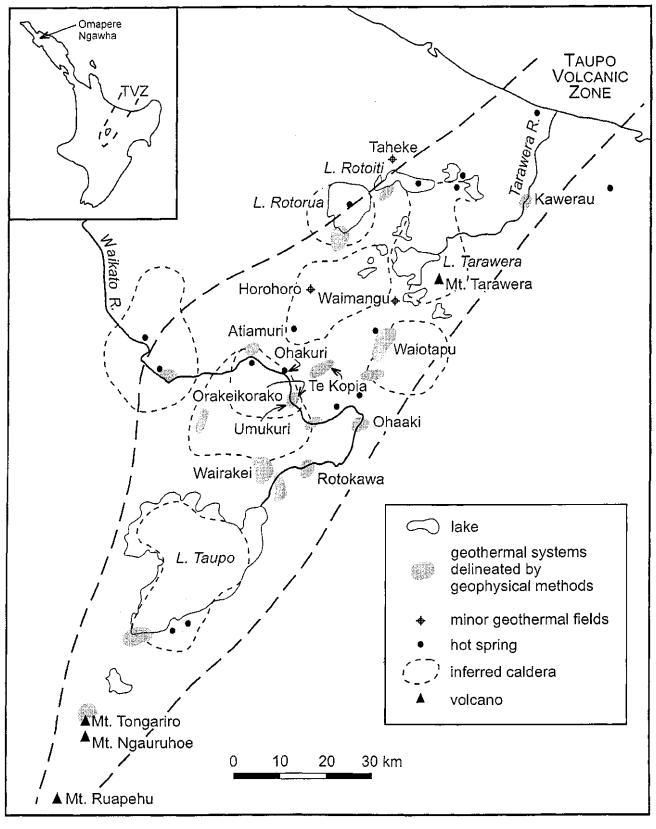

Fig. 1 The Taupo Volcanic Zone, North Island, New Zealand, showing the location of geothermal fields, hot springs and sample sites

Samples

Twenty nine samples of silica sinter were obtained from ten different active and extinct geothermal systems (Table 1). The samples were selected from existing collections of the University of Auckland, Department of Geology, or were specifically collected to provide a range of occurrences and ages of typical thin-bedded sinters (see White et al. 1964. p. B31). Less common textural types and silica residue were excluded. All were deposited from alkali chloride waters. Three consist of deposits from water discharge drains of producing fields, twelve represent active springs with ages of <300 years, eleven are from sinters ranging from 2000 to $<120{,}000$ years old, and three are from Miocene deposits. Twenty one are from geothermal fields of the TVZ (Fig. 1). By way of comparison five samples were examined from fields elsewhere in New Zealand and three from North America. Where single sinter samples showed macroscopic differences such as multiple layers or textural variations, separate analyses were made of each of these different facets.

Silica sinters typically show features that distinguish them from silica residue. These include laminations, ripple and comb structures, dendritic habits, pallisade fabrics, and geyserite. Some sinters contain casts of leaves or twigs, or indeed, in the Te Kopia sample, wood itself. Pollen grains are frequently preserved in sinters and may be examined by standard palynological techniques (e.g. Martin et al. 1999). In contrast, silica residue is a product of leaching by steam condensates and does not produce a deposit with these same characteristics.

The ages of the youngest sinter samples are known since they comprise deposits from thermal features now active (e.g. drain samples, Atiamuri B) or from springs that discharged in living memory (Crow's Nest Geyser, Atiamuri A, Ohaaki Pool.) The silica sinter at Te Kopia surrounded a branch that was dated by C^{14} (Bignall and Browne 1994). The age of the Atiamuri samples are constrained by tephras of known age and the age of the Orakeikorako pit samples was also estimated by tephrochronology.

The ages of the Ohakuri samples are not known with certainty but this geothermal system became extinct about 40,000 years ago and, as such, this age can be taken as a minimum for sinter (Henneberger and Browne 1988). The ages of sinter deposits at Omapere and Umukuri have been estimated from the pollen they contain. The Omapere sample contains pollen from a wide variety of species including some introduced by Europeans 150 years ago. The Umukuri sinter contains pollen of plants that represent an interglacial episode between 40,000 to 120,000 years ago.

Methods used for mineralogical and physical characterisation of the sinter samples are those of Herdianita et al. (in press) and include X-ray powder diffraction (XRPD), thermal analysis (TA), and water, porosity and density analyses. Textural and morphological observations were undertaken with scanning electron microscopy (SEM).

Sample numbers used, prefixed AU, are those of the University of Auckland, Department of Geology, petrology collection.

X-ray powder diffraction results

X-ray powder diffraction (XRPD) results were obtained with a Philips diffraction goniometer fitted with a graphite monochromator with acquisition controlled by Diffraction Technology VisXRD software. Operating conditions were 40 kV at 20 mA, using CuK_α radiation ($\lambda_{\alpha 1} = 1.5405$ Å). Samples of untreated, dry, hand-ground, <106 μm powders, containing an internal

Table 1 Summary descriptions and ages of silica samples studied

AU number[a]	Locality	Geothermal system; sample description	Approx. age (years)[b]	Number of analyses	Silica minerals present	d-spacing (~4 Å line)	Width of ~4 Å line/ band[c] (Δ°2θ)	Other constituents	Water[d] (< 110 °C)	Water[d] > (110 °C)	Particle density (g cm^{-3})	Porosity (%)
AU47276	Wairakei Drain 1	Active, discharge drain; yellow, friable, laminated	0	7	Opal-A	4.04–4.11	7.2–8.2	–	3.2	2.8	2.04	60
AU47277	Wairakei Drain 2	Active, discharge drain; white, dense, thinly banded	0	1	Opal-A	4.02	8.1	–	3.6	4.0	1.64	44
AU47252	Kawerau Drain	Active, discharge drain; black, thinly banded	0	3	Opal-A + quartz	3.92, 4.26	8.3, 0.12	CaNa aluminosilicate(s)	1.6	4.0	2.03	–
AU47243	Atiamuri B	Active, hot spring; white, friable	0	1	Opal-A	4.04	7.3	Plant fragments	3.7	4.1	1.67	55
AU47249	Golden Fleece terrace, Orakei korako	Active, hot spring; white, crumbly, microbial casts	0	1	Opal-A	4.09	6.9	Plant fragments	2.3	2.1	1.94	45
AU47256	Ohaaki Pool	Modified active, hot pool; composite banded overhang,	40	6	Opal-A	4.01–4.27	4.4–7.0	Calcite	2.8 (av)	4.5 (av)	1.93 (av)	30 (av)
AU47248	Crows Nest, Taupo	Extinct, geyser remnant; white, soft, friable, banded	50	2	Opal-A	3.99	7.1	–	3.8	3.6	1.87	55
AU47246	Champagne Pool 1, Waiotapu	Active, hot pool; irregular yellow ripples, white combs	50	2	Opal-C + opal-A	4.04–4.06	0.25, 3.6	Sulfur	5.7 (av)	5.0 (av)	2.04	18
AU47247	Champagne Pool 2, Waiotapu	Active, hot pool; irregular yellow ripples, white combs	50	2	Opal-C + opal-A	4.05–4.07	0.15	Sulfur	4.5 (av)	5.0 (av)	–	–
AU47242	Atiamuri A	Active, hot spring; white, porous, fragmental	60	1	Opal-A	3.95	6.9	–	4.7	4.6	2.02	35
AU47245	Atiamuri SP	Active, hot spring; white to grey, porous, fragmental	60	1	Opal-A	4.04	7.5	–	4.7	4.5	1.91	37
AU47260	Omapere 6	Extinct; white to red to grey, organic-rich, crystalline, hard	150	1	Opal-A	4.02	6.4	Plant fragments	1.8	4.6	2.06	10
AU47261	Omapere 18B	Extinct; soft, stem-rich	150	1	Opal-A	4.13	6.7	Plant fragments	1.8	2.5	2.00	51
AU47262	Omapere 22	Extinct; black organic-rich	150	1	Opal-A	4.06	6.8	Plant fragments	2.4	3.3	2.03	14
AU47263	Omapere 39	Extinct; black organic-rich	?150	1	Opal-A ± opal-CT	4.05	6.7	Plant fragments	2.0	3.1	2.05	11
AU47264	Orakei korako, pit 7 m below Ruatapu	Locally active; white, friable, dendritic	<2000	2	Opal-A	4.04–4.06	6.9–7.0	–	3.2	3.0	1.63	44

AU47266	Te Kopia, northern end of field	Locally active; red and black layers about tree branch	3026 ± 43 B.P.	5	Opal-A + quartz	4.02–4.10	7.4–6.3	–	3.7	3.3	2.03	35
AU47241	Atiamuri 14 (Upper A)	Active; white, crystalline, banded, compact	12,000–15,000	1	Opal-A	4.03	6.8	Plant fragments	1.9	2.1	2.03	10
AU47 39	Atiamuri	Extinct; white, crystalline, banded, compact	>20,000	1	Opal-CT + quartz	4.09	0.70, 0.21	–	2.9	2.0	2.13	16
AU47240	Atiamuri 1	Extinct; white, crystalline, banded, compact	>20,000	1	Quartz	4.26	0.21	Abundant plant fragments	0.4	1.1	2.54	6
AU47255	Ngawha	Active	?10,000–20,000	1	Quartz	4.26	0.13	–	0.0	0.3	2.66	5
AU47258	Ohakuri 48	Extinct; white, granular, glassy	>40 000	1	Opal-A	4.03	7.3	–	5.5	4.5	2.03	4
AU47259	Ohakuri 102	Extinct; white, compact, banded	>40 000	4	Opal-CT	4.08–4.09	0.66–0.69	–	4.2	2.1	2.13	21
AU47271	Umukuri A	Extinct; multiply banded, yellow to white	40,000–120,000	6	Opal-CT	4.09–4.13	0.54–0.69	Plant fragments	3.8 (av)	1.1 (av)	2.54	3
AU47273	Umukuri B upper	Extinct; coarsely banded, greenish white	40,000–120,000	1	Opal-CT + quartz	4.08	0.58–0.68	Plant fragments	4.7	1.2	2.13	7
AU47274	Umukuri B lower	Extinct; milky white, yellow green bands	40,000–120,000	2	Quartz + opal-CT	4.26, 4.05	0.15, 0.75	Plant fragments	0.6	1.0	2.36	18
AU47250	Hasbrouck, Nevada	Extinct; yellow, hard	~10 000 000	1	Quartz	4.26	0.14	Plant fragments potash feldspar	–	–	2.49	3
AU47253	Lincoln, Montana	Extinct; red, very hard	>10 000 000	1	Quartz	4.26	0.16	Plant fragments	0.1	0.6	2.57	4
AU47254	Lincoln, Montana 1	Extinct; laminated, red	>10 000 000	1	Quartz	4.26	0.15	–	0.2	1.0	2.57	4

[a] AU number indicates University of Auckland, Geology Department, petrology collection
[b] Age estimates are those of the samples, not necessarily of the geothermal fields; see text
[c] Width of ~4-Å line/band at half-maximum intensity, $\Delta^\circ 2\theta$, as defined by Herdianita et al. (in press) from oven drying of sample for 12 h at 110 °C
[d] From Penfield determination less value given in footnote c.

silicon standard, and mounted in the standard aluminium holders were scanned at 0.6°2θ min^{-1} from 10–40°2θ, with a step size of 0.01° (Herdianita et al. in press).

Silica phases

X-ray powder diffraction traces of the sinters showed patterns of opal-A ± opal-CT ± opal-C ± quartz ± non-silica species (Fig. 2). The width at half-maximum intensity of the distinctive ~4 Å diffraction line or band is tabulated in Table 1 and is taken here as a guide to the relative degree of lattice order or disorder within each of the silica species (Herdianita et al. in press).

Noncrystalline opal-A of the sinters is typified by a very broad band of moderate intensity centred about 3.90–4.13 Å (Fig. 2a) with an additional weaker band sometimes present near 2.4 Å (see Jones and Segnit 1971; Smith 1998). The broad ~4 Å band typically has a raw intensity of less than 110 counts s^{-1} under the operating conditions used typical of noncrystalline opal-A (see Flörke et al. 1991). This pattern is seen in sinters known to be young such as those from Wairakei, Orakeikorako and Crows Nest. Subdued lines of quartz, probably of detrital origin, occur at 4.26 and 3.34 Å in some patterns that are otherwise dominantly opal-A, e.g. Kawerau and Te Kopia (Martin et al. 1999).

Thirty eight analyses of 19 samples of opal-A silicas showed band widths ranging 6.3–8.3°2θ (1.60–1.25 Å) with a mean of 7.3 ± 0.5°2θ (1.33 Å). The maximum value is shown by one of the siliceous layers from the Kawerau drain and the minimum by Ohakuri sample 48.

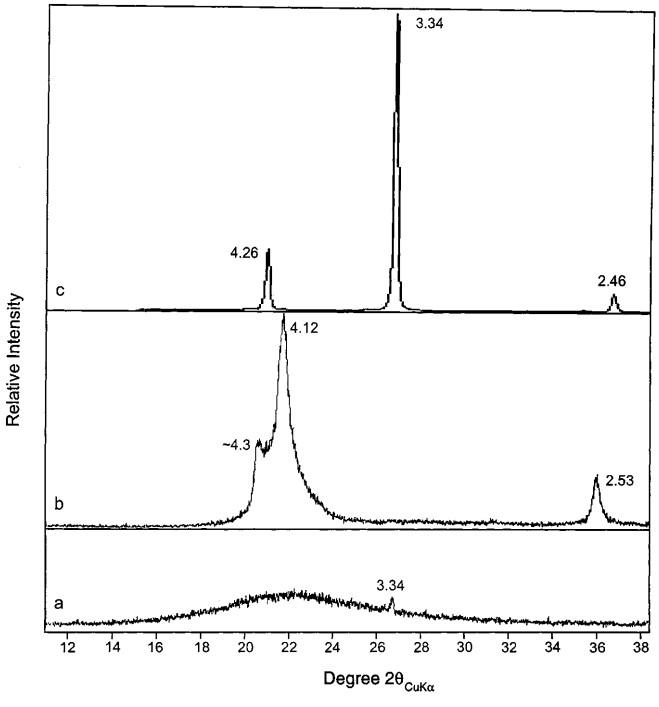

Fig. 2a–c Typical X-ray powder diffraction traces of siliceous sinters of different ages. **a** Noncrystalline opal-A, Wairakei showing a trace of quartz; **b** paracrystalline opal-CT, Umukuri, showing some limited structural ordering with broad diffraction lines at 2.53 and 4.12 Å, with shoulder at about 4.3 Å; **c** quartz, Umukuri, with characteristic (1 0 0) and (1 0 1) diffraction lines at 4.26, 3.34 and 2.46 Å

Paracrystalline opal-CT and opal-C. Silica sinters ranging in age from 50 to 40,000 years, such as those from Atiamuri and Ohakuri, yielded powder diffraction patterns typical of partially ordered opal with a variable proportion of cristobalitic- and tridymitic-like stacking sequences (see Smith 1998). Strong, but moderately broad, diffraction lines occur from 4.12–4.04 Å with a shoulder, centred at about 4.3 Å (Fig. 2b), typical of opal-CT (e.g. Jones and Segnit 1971; Smith 1997). This is in distinct contrast to the "hydrothermal β-cristobalite" which "normally lacks a tridymite shoulder" that was reported to be a major component of older sinters from Steamboat Springs (Nevada), Yellowstone (Wyoming), and Orakeikorako (New Zealand), by White et al. (1988, pp. 8–9). No such β-cristobalite pattern lacking a 4.3 Å shoulder was found in the present study (see Jones and Segnit 1971). Up to eight additional broad lines may be present in the pattern of opal-C but the only one readily seen is that of opal-CT – at 2.5 Å. The ~4-Å opal line of these sinter specimens typically has a raw intensity approximately six times that of opal-A, except for sinters from Champagne Pool which showed intensities half that of typical opal-A. Weak, but diagnostic lines of quartz were noted in some traces, such as samples from Atiamuri and Champagne Pool.

There is an abrupt decrease in the width of the ~4-Å line in these paracrystalline opaline silicas compared to the corresponding band in opal-A dominant sinters. Opal-CT in five samples (14 analyses) ranges from 0.5–1.7°2θ (0.16–0.05 Å) with a mean of 0.7 ± 0.4°2θ (0.14 Å). By contrast opal-C, found in only two samples (four analyses), had a ~4 Å line width of 0.4°2θ (0.04 Å).

Quartz dominates the diffraction patterns of sinters from Ngawha (NZ), Lincoln (Montana), Hasbrouck (Nevada) and Atiamuri 1 (N.Z.), all of which are among the oldest deposits studied (Fig. 2c). Texturally, these rocks comprise microcrystalline quartz and the widths of all the (100) diffraction lines at 4.26 Å were ~0.15°2θ (0.03 Å).

The quartz crystallinity indices (CI), as defined by Murata and Norman (1976), are shown in Table 2 for

Table 2 Crystallinity index (CI) of quartz (Murata and Norman 1976) in silica sinters (see text)

Sample	Silica minerals		CI
Kawerau drain	Bulk	Detrital quartz + opal-A	4.6
Atiamuri 1	–	Quartz	1.6
Umukuri A		Opal-CT + quartz	2.0
Umukuri B	Upper	Opal-CT + quartz	2.1
	Bottom	Quartz + opal-CT	3.2
Ngawha	–	Quartz	10.1
Hasbrouck	–	Quartz	7.2
Lincoln	–	Quartz	5.0
Lincoln 1	–	Quartz	4.6

each of the sinters. The Ngawha sinter has the highest value with an index of 10. In contrast, the Lincoln, and Hasbrouck quartz-rich sinters have indices of 5–8. Younger sinters, such as Umukuri and Atiamuri, where quartz was a minor component of the samples studied, have CIs ≤3.

This crystallinity index for quartz shows a close but non-linear relationship with the width of the 4.26 Å diffraction line, although as the quartz CI decreases markedly from 10 to near 3, the width of the 4.26 Å line increases by only 0.1 °2θ.

Other mineral phases

All the older quartz-bearing sinters showed a small Raman scattering band at 499–505 cm^{-1} (Herdianita et al. in press). Kingma and Hemley (1994) demonstrated that this band is consistent with the presence of the metastable transitory silica polymorph moganite in microcrystalline silica samples. The abundance of this species is presumably insufficient for its diffraction lines to be above background in routine X-ray diffraction scans.

The characteristic diffraction lines of native sulfur occur in the powder diffraction patterns of sinters from Champagne Pool and those of calcite in sinter patterns from the Ohaaki Pool. Anhydrite, natroalunite and alunite are also associated with Champagne Pool sinter, potash feldspar with Hasbrouck, and an unidentified calc-aluminosilicate is present in the pattern of the Kawerau drain deposit.

Morphology and microtextures

Examination of the sinters by scanning electron microscopy (SEM) was undertaken using a Philips 505 instrument, retrofitted with a lanthanum hexaboride (LaB_6) filament. The accelerating voltage varied from 15 to 20 kV.

Four principal silica morphologies are present (Figs. 3, 4): (1) spherical aggregates of opal-A; (2) dense vitreous silica; (3) lepispheres and amygdaloidal (almond-shaped) clusters of opal-CT and/or opal-C; and (4) quartz microcrystals. Opal-A spheres form early in the history of hot spring silica deposition, whereas quartz is a late stage silica phase. The other characteristic silica morphologies develop in the interval between formation of these two end-members.

Young silica sinters typically consist of spheres of opal-A and, in places, contain laminated fabrics with silicified plant fragments or microbial moulds. The spheres are most commonly 4–8 μm in diameter but some are smaller, in the range of 1–2 μm in diameter (Fig. 3a). Larger, globular aggregates, 8–10 μm diameter, are common (Fig. 3b), as are spherical particles connected in chains, from 5 to 150 μm long (Fig. 3c). In the Te Kopia and Kawerau sinters, such composite grains may be coated by a thin, smooth layer of non-crystalline secondary opal-A (Fig. 3d) which partially obscures textural detail. Some sinters, such as at Omapere, show close packing of the silica spheres and early silicification of plant fragments (Fig. 3e). External moulds of spinose spores also are preserved in plant-rich sinters (Fig. 3f). In addition, Omapere sinter displays a thin, irregularly banded microtexture that formed around plant fragments prior to their decomposition (Fig. 3g). Smooth, dense vitreous silica later may fill such plant moulds (Fig. 3h). Other sinters, such as at Hasbrouck, contain a different type of layered fabric comprised of very thinly laminated (1–6 μm thick) dense silica horizons alternating with vertical palisades of filament-like structures (Fig. 4a). Similar palisade fabrics in sinters have been interpreted elsewhere to have developed in association with microbial mats (Walter et al. 1996, 1998; Jones et al. 1998). Detailed views of silicified filaments from Ohaaki sinters (Fig. 4b, c) reveal somewhat granular outer textures and rare hollow centres (Fig. 4c; see Jones et al. 1997, their Fig. 5D–I, p. 93). Hence, young silica sinters preserve textures that reflect the initial aggregation and growth of opal-A spheres and chains. Organic materials (plants, filamentous microbes), where present, facilitated development of early formed, laminated fabrics.

Older sinters rich in opal-CT and/or opal-C, such as from Umukuri, typically contain lepispheres, which are spherical, microbotryoidal clusters, <10 μm in diameter, formed of thin-bladed crystals that appear to pseudomorph the original opal-A spheres (Flörke et al. 1975; Fig. 4d). This microtextural change is accompanied by the abrupt reduction in the width of the ~4-Å diffraction line at half-maximum intensity, from 6–8°2θ (1.6–1.25 Å) in the opal-A dominant sinters, to 0.5–1°2θ (0.16–0.06 Å). In some sinters, as at Umukuri, lepispheres co-occur with finely fibrous, amygdaloidal clusters of opal-CT, 20–30 μm across (Fig. 4e). Anhedral to euhedral quartz typifies ancient sinter samples. Textural relationships, shown by SEM examination, suggest that initial crystallisation toward quartz took place with the growth of anhedral microcrystals, <5 μm long parallel to the c-axis, upon the surface of opalCT (Fig. 4d, seen as irregular aggregates that surround lepispheres). Similarly sized, but euhedral microcrystals have developed as parallel and rare rosettes epimorphously grown upon broken conchoidal and corroded surfaces (Fig. 4f, g). These quartz habits display a low CI of ~2. Late stage quartz crystals, with a CI of 5–7 and up to 30–50 μm along c, occur as drusy linings in cavities or infilled fractures (Fig. 4h). Commonly, these crystals are <100 μm in length but those from the Atiamuri and Lincoln sinters are up to 300 μm long.

Some hot springs deposit mineral phases other than silica. For example, silica-encrusted calcite microcrystals, 15–30 μm long and <1 μm diameter, and rare 10 μm calcite scalenohedra are associated with particles of silica from the Ohaaki pool (Jones and Renaut 1996).

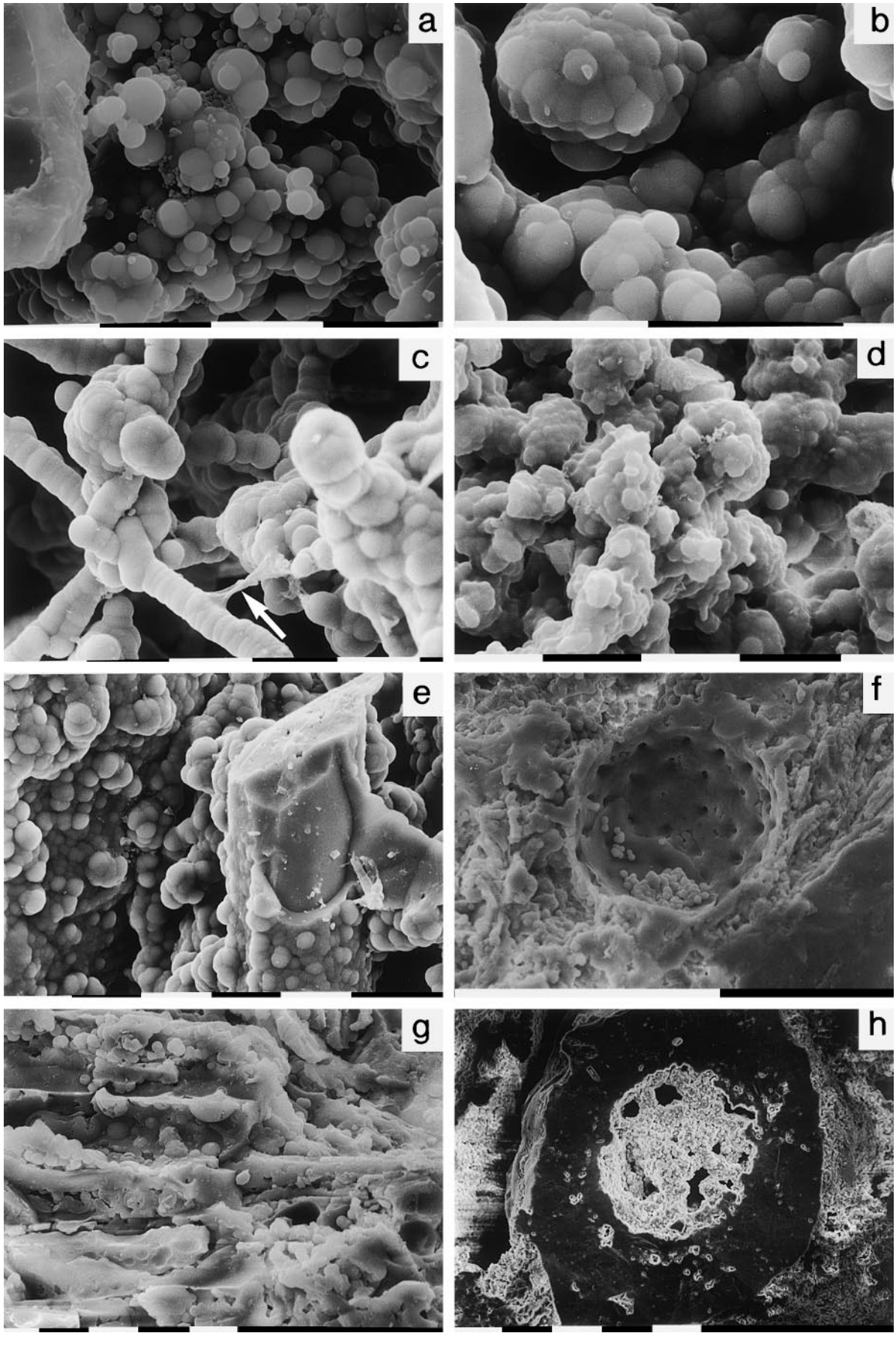
a
b
c
d
e
f
g
h

◄

Fig. 3a–h SEM photomicrographs of opal-A microtextures. **a** Typical 4–8 μm diameter spheres with smaller 1–2 μm diameter spheres, Wairakei Drain (*scale bar* 10 μm); **b** spherical aggregates 8–10 μm across, Wairakei Drain (*scale bar* 10 μm); **c** twisted chain-like aggregates (to >40 μm length), of uncertain origin, with attached ?mucus string (*arrow*), Omapere (*scale bar* 10 μm); **d** aggregate spherical grains coated by a thin, smooth layer of dense secondary silica, Te Kopia (*scale bar* 10 μm); **e** close packing of the silica spheres (*left background*), with silicified plant fragment (*right foreground*) encrusted by coating (2–4 μm thick) of cemented silica spheres, Omapere (*scale bar* 10 μm); **f** external mould of spinose plant spore (~80 μm across), with small pile of silica spheres (~2 μm diameter) as geopetals on spore mould surface, Omapere (*scale bar* 0.1 mm); **g** irregularly layered fabric (on the order of ~10 μm thick) produced by silicification around plants prior to their decomposition, with opal-A spheres and sphere impressions apparent, Omapere (*scale bar* 10 μm); **h** cross section of plant stem mould (0.6 mm diameter), infilled with dark, dense vitreous silica, Omapere (*scale bar* 0.1 mm)

Thermal analytical behaviour

Samples were analysed using a Rheometric Scientific Simultaneous Thermal Analyzer STA 1500 capable of simultaneous determination of differential thermal analytical (DTA) and thermogravimetric (TG) profiles of samples. A sample weight of 15.0 ± 0.1 mg of <106 μm powder was heated at a rate of 20 °C min^{-1} in an atmosphere of dry air (Herdianita et al. in press). Where organic matter was present in a sample, thermal profiles made in a nitrogen atmosphere proved helpful in distinguishing different thermal events. The system was calibrated against the melting point of 99.999% KCl.

Examples of characteristic DTA responses of the sinters are shown in Fig. 5. Noncrystalline, opal-A dominant sinter from the Wairakei drain shows a broad, progressive, endothermic release of adsorbed water below 200 °C. At about 1200–1300 °C, a distinct, sharp, exothermic event is recorded upon crystallisation of cristobalite (Fig. 5a). The β → α inversion of cristobalite occurs on cooling near 200 °C. Reheating shows its expected reversal. In contrast, the sole exothermic reaction recorded in the thermal profiles of the Atiamuri, Atiamuri 14, Ohakuri 48, Omapere and Te Kopia sinters heated in air resulted from combustion of their organic contents (Fig. 5b), although a β → α cristobalite inversion at ~200 °C was evident upon cooling.

The temperature of the β → α cristobalite inversion increases with an increase in structural ordering of silica (Smykatz-Kloss 1974). The young opal-A sinters reveal a β → α cristobalite inversion ≥190 °C, e.g. sinter from Orakeikorako at ~210 °C and the Wairakei drain at 190 °C. Sinters 10,000–50,000 years old, and comprised mainly of paracrystalline opal-CT and/or opal-C, such as those from Umukuri and Ohakuri, displayed inversions near 150 °C. In general, young sinters in which silica is associated with other mineral phases, show β → α cristobalite inversions near 150 °C.

Samples with >5% organic matter, such as the Omapere sinter, record an intense, broad combustion exotherm, with a maximum from 250 to 350 °C (Fig. 5b). In these cases, DTA baseline drift was marked, and, in order to estimate the intensity of the organic combustion event the DTA trace recorded in nitrogen was subtracted from that obtained in air from the same sample. Where two distinct TG weight losses are registered, they have been assigned here to dehydration and combustion events.

Samples from Atiamuri 1, Ngawha, Hasbrouck and Lincoln display the characteristic α → β inversion of quartz in the range 550–580 °C (Fig. 5c). This inversion is not observed on cooling of samples that became partially vitrified when heated above 1000 °C (White and Grimshaw 1970). Thermogravimetry yielded a <1 wt% weight loss from quartz-rich sinters heated to 1450 °C under atmospheric conditions.

The presence of alunite in both sample Ohakuri 22 and the soft white layer from Atiamuri RD was confirmed by endothermic reactions at 553 and 745 °C (Fig. 5d), which are characteristic of this mineral (Smykatz-Kloss 1974). As expected from its XRPD trace, the exothermic combustion of sulfur at ~300 °C was observed in the Champagne Pool sinter. Calcite decomposed between 750–800 °C in the Ohaaki Pool sinter and minor pyrite oxidised at ~450–550 °C in a sample of the Kawerau drain deposit.

Water contents

The importance of water content in characterising different silica phases has been summarised and stressed by Flörke et al. (1991) and Graetsch (1994). A distinction is made between molecular water (H_2O_{mol}) and silanol (H_2O_{SiOH}) groups in the structure. Both molecular water and silanol group water are divided into type A (isolated molecules and hydroxyl groups trapped in the structure) and type-B (strongly hydrogen-bonded accumulations of water molecules or hydroxyls either within the structure or on external and internal surfaces). Much of the water in opaline silicas is molecular with the majority of any silanols present being type-B.

Precise determinations of the type and structural environment of water and hydroxyl groups can be made only with infrared and near infrared spectroscopic study (Flörke et al. 1991). However, general trends related to the crystal chemistry and textures of silica sinters can be obtained by more conventional water analyses. Herdianita et al. (in press) have demonstrated that useful information on water contents can be elicited from TG profiles although the resulting value for total water does not always match that from standard Penfield determinations (e.g. Groves 1951). Except for silica sinters from the Champagne and Ohaaki Pools, most silica sinters have <10 wt% total Penfield water.

Low temperature surface-absorbed water

On overnight drying at 110 °C, older, quartz-rich sinters, such as those from Lincoln and Atiamuri, lost

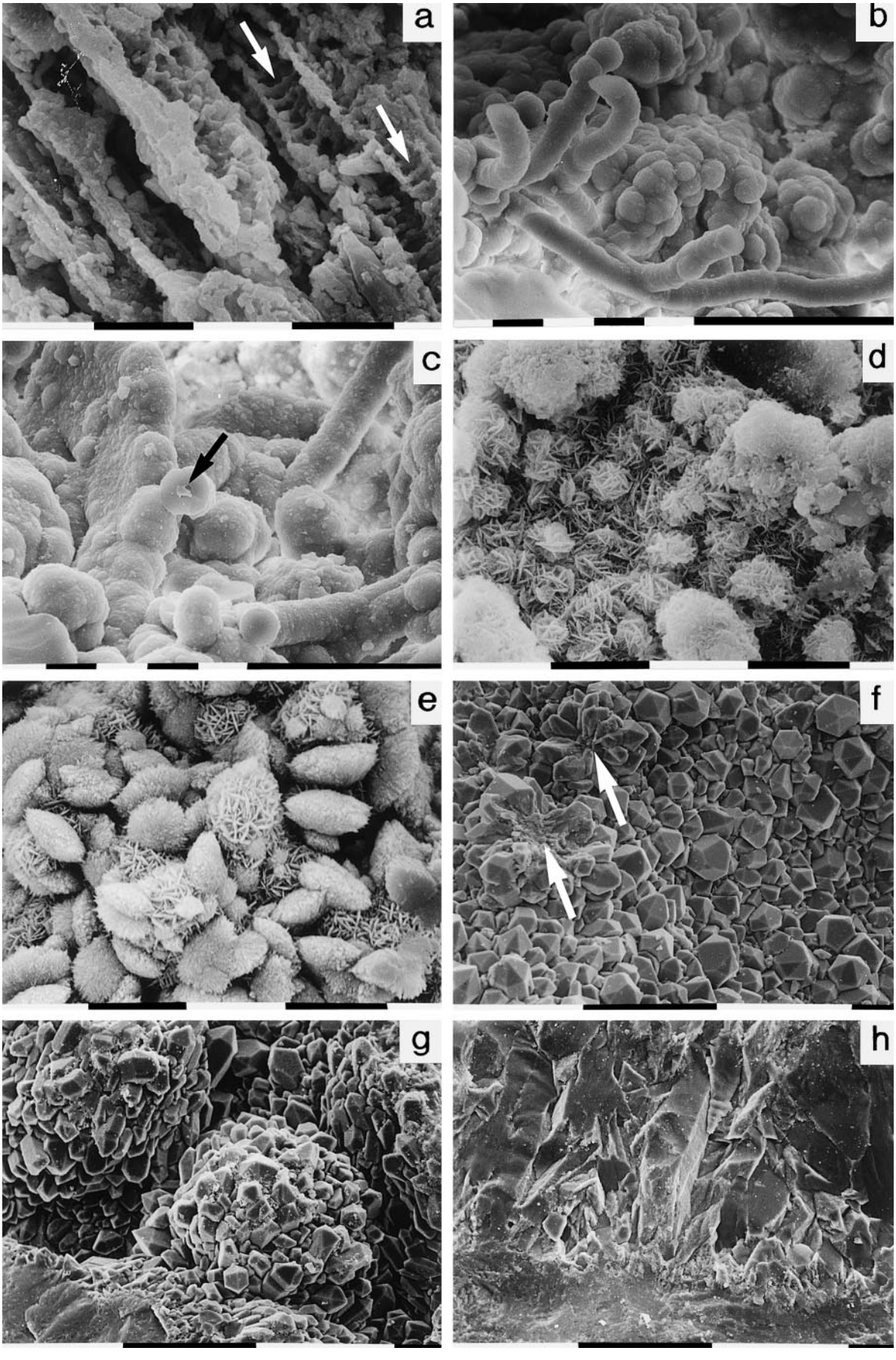
a
b
c
d
e
f
g
h

◄
Fig. 4a–h SEM photomicrographs of opal-A, opal-CT, opal-C and microcrystalline quartz microtextures: **a** very thin layers (1–6 μm thick) of dense silica horizons alternating with vertical palisades of filament-like (?microbial) structures (*arrowed*), Hasbrouck (*scale bar* 10 μm); **b** granular silicified, non-branching filaments, to >100 μm long, of microbial origin, Ohaaki Pool (see Jones et al. 1997) (*scale bar* 10 μm); **c** granular, silicified, non-branching microbial filaments, to >30 μm long, with rare hollow centres (*arrow*), Ohaaki Pool (*scale bar* 10 μm); **d** spherical, microbotryoidal clusters, <10 μm diameter, formed of thin-bladed crystals of opal-CT (lepispheres), surrounded by larger, irregular microcrystals, Umukuri (*scale bar* 10 μm); **e** platy lepispheres with possible overgrowths of fibrous, amygdaloidal clusters of ?opal-CT, 20–30 μm across, Umukuri (*scale bar* 10 μm); **f** euhedral crystals of quartz developed as rosettes (*broken interiors arrowed*) upon existing, conchoidal fractured and corroded quartz surfaces, Atiamuri (*scale bar* 0.1 mm); **g** detail of two quartz microcrystal rosettes, ~130 μm across, Umukuri (*scale bar* 0.1 mm); **h** well-developed, coarse quartz crystals, to 0.2 mm length, in cavity, Umukuri (*scale bar* 0.1 mm)

<0.5 wt%, presumably from loss of adsorbed water. On the same basis, fresh opal-A dominant sinters from drains at Wairakei and Kawerau and some from Omapere, Ohakuri and Atiamuri show 1.5–4 wt% adsorbed water loss, whereas samples from Champagne Pool contain >5 wt% adsorbed water. No natural silica sinter contained >6 wt% adsorbed water.

The corresponding weight losses recorded for the same sinters up to 125 °C by TG are generally lower, except for older sinters that lost up to 0.5 wt%. Other sinters, excluding those from Champagne Pool and Ohakuri 102, lost between 0.5 and 2.5 wt%; Ohakuri 102 lost 2.5–3.5 wt% and Champagne Pool sinter 3 wt%. The contrast between the TG and oven results is believed to reflect the protracted, essentially static nature of the oven analysis compared with the 6 min maximum, experienced by a sample heated over the same temperature range in the dynamic environment of the thermal analyser. Water molecules are absorbed onto a range of sites with wide variation in bonding efficacy. The rate of the dehydration process is such that insufficient energy is available to ensure release of the full complement of absorbed waters in the brief time taken to span the range to 110 °C of a TG analysis.

Higher temperature water

As expected, the TG weight loss increases as the amount of total water increases but there is no exact correlation. For silica derived from sinter largely devoid of other mineral and organic components, the TG weight loss is generally higher than the amount of Penfield-determined water by a factor of up to 1.5. For sinters containing other thermally active constituents, such as sulfur or carbon, the weight loss is markedly greater, as expected. During heating, the weight loss of older quartz-rich sinters tends to remain nearly constant and <2 wt%.

Sinters from the Ohakuri, Atiamuri, Omapere, Te Kopia, and the Wairakei and Kawerau drain sites contain 2–6 wt% Penfield-determined water and have TG weight losses of 2.5–10 wt%. Sinters with total TG weight losses of >10 wt%, such as from Champagne and Ohaaki Pools, contain only 4–6 wt% Penfield-determined water, with the remainder of the loss arising from combustion of organic matter.

Variation in water contents with silica lattice order/disorder

The variation in total Penfield water contents with respect to silica lattice order/disorder is illustrated in Fig. 6 and shows two data clusters that reflect their

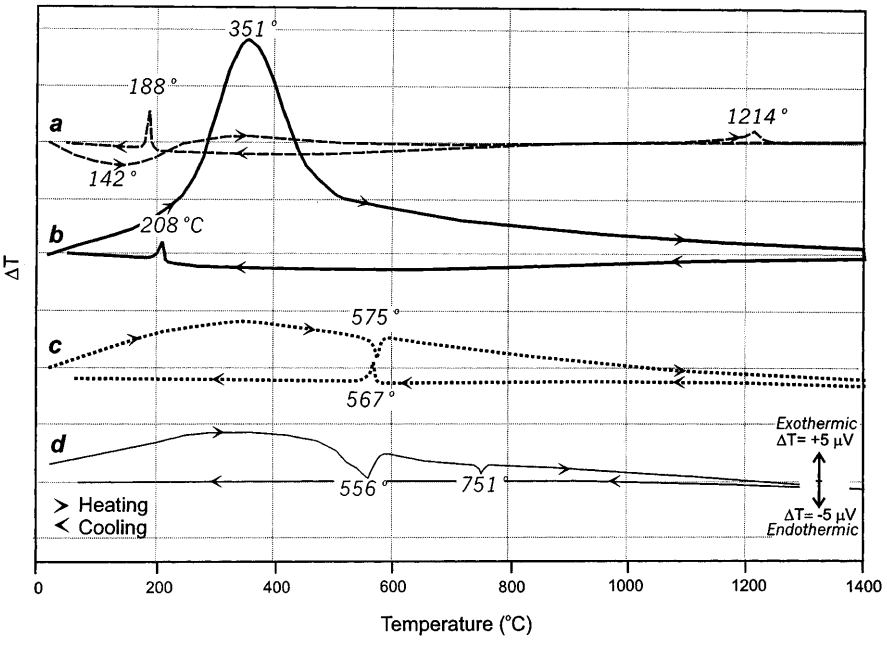

Fig. 5a–d Examples of characteristic DTA responses of the sinters: **a** opal-A sinter from the Wairakei drain showing a broad, endothermic release of adsorbed water below 200 °C and a distinct exothermic event at about 1214 °C recording the crystallisation of cristobalite. The β → α inversion of cristobalite is evident in the cooling trace at 188 °C; **b** the sole exothermic reaction in the heating profile of the Omapere sinter records combustion of its abundant organic content; **c** the characteristic α–β inversion of quartz at 575 °C is shown in the heating trace of the Ngawha sinter; **d** alunite in Ohakuri 22 is shown by endothermic events recorded at 556 and 751 °C in the heating trace

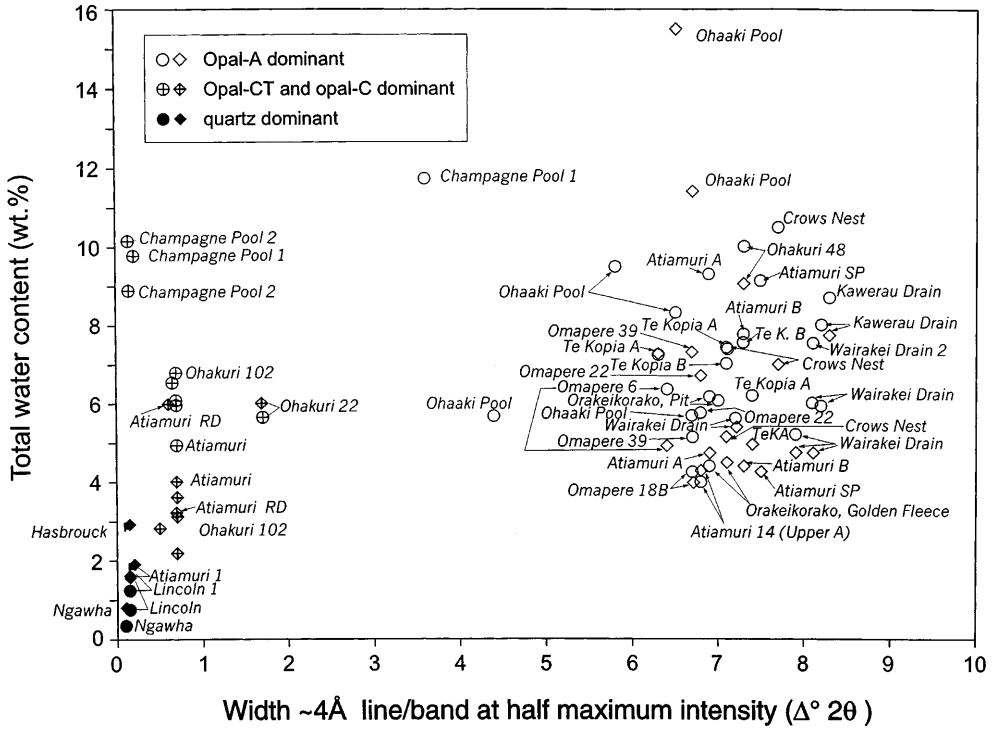

Fig. 6 Variation in total water content with width of the ~4 Å diffraction line or band at half maximum intensity of silicas given in Table 1 (Δ°2θ). *Circles* indicate Penfield-determined water; *diamonds* TG-determined water

bimodal nature. Silicas that have a ~4 Å band/line half-width of <1°2θ contain between 0.5 and 9 wt% total water. With increasing line/band width, water contents generally increase. Sinters with widths of ~6–9°2θ mostly contain 4–11 wt% water. Further, lower-temperature absorbed water may range up to 6 wt%, with the amount of higher-temperature water decreasing to 1–4 wt% with increased lattice ordering. An exact correlation between water content and lattice type is not possible in the absence of infrared spectroscopic study (see Graetsch 1994).

Particle density and porosity

Particle densities and porosity measurements were determined according to standard methods (e.g. Battey and Pring 1997) and are summarised in Table 1. As porosities decrease to <10%, particle densities increase from 2.30 to 2.57 g cm^{-3}. Young sinter rich in opal-A has particle densities of 1.5–2.2 g cm^{-3} and porosities of 10–60%. By contrast, older quartz-rich sinters, such as those from Lincoln and Ngawha, have grain densities of ~2.57 g cm^{-3}, close to that of pure quartz (2.65 g cm^{-3}), and porosities of <6%.

A plot of particle density versus ~4 Å line width of all silica species (Fig. 7) shows that the noncrystalline opaline sinters with a band width of 6–9°2θ have particle densities of 1.5–2.1 g cm^{-3} and porosities of <60%. Samples with enhanced ordering have particle densities of 2.1–2.6 g cm^{-3} and porosities of <30%. Lower densities (and higher porosities) are generally characteristic of sinters with small amounts of opal-CT and opal-C, whereas the higher densities (and lower porosities) are typical of quartz-dominant sinters. The seemingly abrupt jump that occurs in the present samples, in line width from ~6.5°2θ to ~0.6°2θ is not marked by any matching change in density which remains in the range 2.0–2.1 g cm^{-3} during this transition.

Water loss accompanies the increase in particle density and decrease in porosity. Silica sinters with more than 4 wt% total Penfield water have particle densities of <2.2 g cm^{-3} and porosities of 10–60%. Samples with total water contents of <2 wt%, have particle densities up to ~2.6 g cm^{-3} and porosities lowered to ~6%. These variations also are reflected in the amount of both adsorbed and bonded waters.

Discussion and conclusions

The analytical results presented here demonstrate that regular changes in mineralogy and texture occur in silica sinters with time. These observed variations are not products of primary deposition. Whatever conditions may have resulted in subsequent changes to these sinters, none of the New Zealand examples have suffered significant burial. They persist as surface features (see White et al. 1988). The grab sampling strategy adopted in this study limits interpretation of the data in detail. For example, local variations in individual sinters render specific textural or density comparisons from this study of uncertain value. Nonetheless, some novel general trends are apparent.

As the sinter ages the silica species it is composed of changes from noncrystalline opal-A through paracrys-

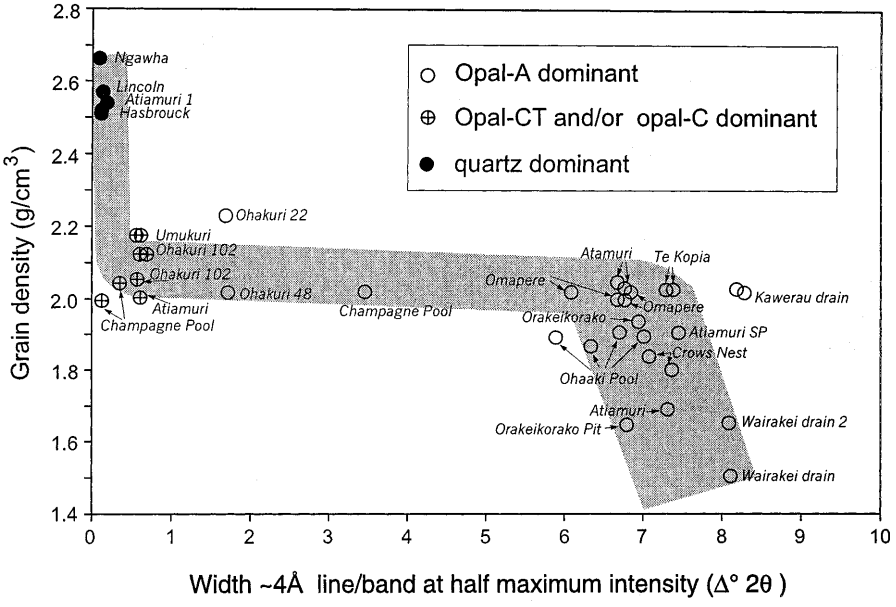

Fig. 7 Variation in particle density with width of ~4 Å diffraction line or band at half maximum intensity of silicas given in Table 1 (Δ °2θ)

talline opal-CT and/or opal-C to microcrystalline quartz. This development is reflected by increases in structural ordering and density, and by decreases in water content and porosity. These same time-dependent trends of evolving crystallinity have also been recorded from microscopic opals in marine sediments (e.g. Murata and Nakata 1974; Kano 1983) and in Quaternary sinters at Steamboat Springs, Nevada, (White et al. 1964) and Norris Basin, Yellowstone, (White et al. 1988).

In Fig. 8 the width of the ~4 Å X-ray line or band at half maximum intensity is plotted against the probable age of the sample. While the variations in width can give an approximate guide to the relative degree of crystal lattice order (or disorder) within each of the silica species, care needs to be exercised in making any comparisons between the diffraction responses obtained from the noncrystalline, paracrystalline and crystalline silicas. With each phase, different quantities are being compared. The broadening of lines produced by Bragg reflections from, say, quartz result from imperfections in the long range order of the lattice such as is typical of quartz formed by recrystallisation as here (Smith 1997). In opal-CT and, to a lesser extent in opal-C long range order is restricted, and line width variations are primarily determined by the range in size of the minute, coherently scattering crystallite domains. The broad

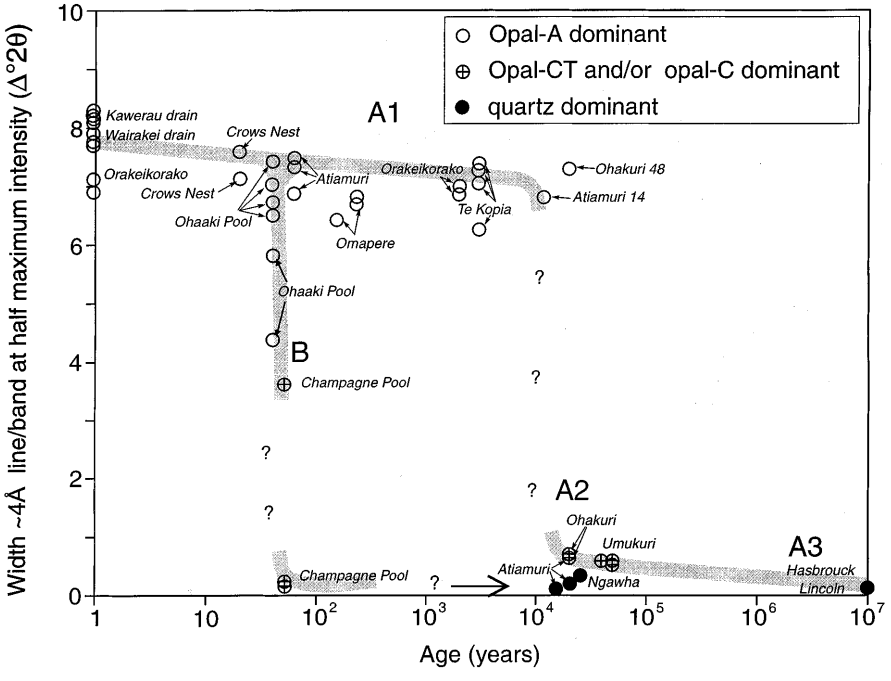

Fig. 8 Variation in the width of ~4 Å diffraction line or band at half-maximum intensity with age of the different silica phases given in Table 1 (Δ°2θ). *Trend A* is for samples with >95% SiO_2; *A1* for sinters that are dominantly opal-A, *A2* for sinters dominated by opal-CT and opal-C, and *A3* for quartz-rich sinters. *Trend B* indicates samples containing significant amounts of other mineral species or plant remains

band response from opal-A indicates a general absence of any long range order and it is assumed here that differences in band width of these noncrystalline opals indicate differing extents of disorder between samples. This caveat aside, two trends are apparent in Fig. 8, both of which point to time dependent changes.

The typical, first deposited, spherical particles of opal-A, as in the Wairakei drain, have an ~4 Å band width at half-maximum intensity of 6.3–8.3 °2θ (1.6–1.3 Å). Subsequently, as these particles aggregate and become more closely packed (e.g. Omapere) and enveloped in a film of thin secondary silica, there is a slight decrease in band width to ~5.8°2θ (~1.2 Å). This shift occurs over ~10,000 years for sinters largely devoid of other minerals or other materials such as plant remains (Fig. 8, trend A1). Over the next ~10,000 years, the noncrystalline silica progressively crystallises to poorly-ordered opal-CT and eventually to opal-C. Bladed lepispheres of opal-CT replace the opal-A particles. Microbotryoidal aggregates are common (e.g. Fig. 4b). The half-width of the ~4 Å line of these new silica phases is reduced to 0.4–1.7°2θ (0.16–0.04 Å) as the degree of disorder in each is reduced (Fig. 8, trend A2); the lower value being close to that seen in the oldest, quartz-rich sinters.

The difference in response of the primary X-rays to the extent of long range order in the silica analytes is seen in the seemingly abrupt jump that occurs between trend A1 and trend A2 in Fig. 8. Once appreciable long range order develops in a silica phase the incident beam responds far more sensitively than when short range order predominates. Such a change in ordering would not be expected to have any expression in the density measurements, as proved to be the case.

Flörke et al. (1991) demonstrated that paracrystalline opal shows a decrease in the d-spacing of the maximum intensity of the ~4 Å diffraction line with an increase in structural ordering. Among the sinters studied, this correlation is somewhat poorly defined. Except for samples from the Ohaaki Pool, the variations in d-spacing at maximum intensity of this line is ± 0.10 Å for those deposits $< 50{,}000$ years old. Mizutani (1977) observed that changes in d-spacing of microcrystalline opal upon recrystallisation are largely determined by the thermal history experienced by silica following deposition. This shift suggests that under different conditions of preservation, silica sinter may well show significant, albeit small changes in the d-spacing of opal-CT, as is observed for samples of Umukuri sinter. Perhaps at Umukuri, sinter remained hot after deposition owing to heat conduction. The majority of other sinter samples, which have been preserved under apparently similar surface environments, indicate little variation in d-spacing of the ~4 Å line upon transformation from opal-A to opal-CT or opal-C. All sinters older than 50,000 years have largely recrystallised to microcrystalline quartz with the d-spacing of the (100) reflection at 4.26 Å (Fig. 8, trend A3).

Progressive changes in sinters with age also are apparent from trends in loss of adsorbed water, increase in particle density, and decrease in porosity. Young opal-A sinter, with a particle density of 1.5–2.1 g cm^{-3}, contains 4–10 wt% low-temperature adsorbed water, and its porosity ranges from 35 to 60%. Over 10,000 to 20,000 years, with crystallisation of opal-A to opal-CT and/or opal-C, the water content falls to < 7 wt%, comprising < 5 wt% low temperature adsorbed water and ~2 wt% Penfield water. Over the same interval, the particle density increases to ~2.3 g cm^{-3} and porosity drops to $< 30\%$. With the onset of quartz crystallisation after ~20,000 years, most adsorbed water is lost, but some water/hydroxyls remain. Tertiary sinters, e.g. the samples from Hasbrouck and Lincoln, contain no more than 1 wt% water, of which < 0.2 wt% is adsorbed. In these older samples, the particle density is near that of quartz (2.65 g cm^{-3}) and porosity has dropped to $< 4\%$.

Changes in silica species and ordering occur earlier where the sinters contain appreciable amounts of other materials (e.g. calcite, organic remains), as for example at the Ohaaki and the Champagne Pools (Fig. 8, trend B). It would appear that the presence of such substances facilitates silica recrystallisation, as was noted by Rimstidt and Cole (1983). The present results suggest that in sinters with mineral or organic inclusions, opal-A may pass to opal-C in less than 50 years but without opal-CT necessarily appearing as an intermediate phase. However, other factors can also be involved in catalysing the (re)crystallisation processes. These include the temperature of initial deposition and the post-depositional history of the sinter, including any heating it may have undergone. For example, Martin et al. (1999) noted that a circa 3500 B.P. sinter from Te Kopia, which is predominantly opal-A, has converted to opal-CT where it has been heated by adjacent fumaroles.

An apparent decrease in the porosity of samples from Ohaaki and Champagne Pools arises from the co-precipitation or later precipitation of calcite. For certain Omapere samples (6, 22, 39), a porosity of ~10% may reflect silicification of included plant fragments.

Silica microtextures and silica species types also change with sinter ageing (Figs. 3, 4). Opal-A spheres form in silica-saturated hot-spring fluids, wherein polymerisation promotes growth and precipitation of colloids; these colloids aggregate to form a friable, porous, weakly cemented deposit (Iler 1979; Rimstidt and Cole 1983; Fournier 1985; Everett 1994), such as occurs in young sinters (e.g. Wairakei Drain; Fig. 3a, b). Agglomeration of spheres may be catalysed by the presence of organic matter (Rimstidt and Cole 1983), as for example the Omapere sinter and at Ohaaki Pool (Figs. 3e–g, 4b, c). Even in older sinters that have recrystallised to quartz, some original microtextures can be preserved that formed in association with organic matter, such as the fossil microbial filaments in the Miocene Hasbrouck sinter (Fig. 4a). However, in many ancient sinters such primary fabrics are substantially modified or even destroyed by late quartz recrystallisation and growth of cements (Walter et al. 1996, 1998).

Determining the origin of particular sinter microfabrics can be difficult, especially for elongate chain- or bead-like aggregates (e.g. Figs. 3c, 4b, c), because these chains can form inorganically by colloidal processes and flocculation (Iler 1979; Everett 1994), or by silica encrustation of microbial filaments (e.g. Jones et al. 1997, 1998; Cady and Farmer 1996; Walter et al. 1996, 1998). In this study, the presence of granular outer surfaces on palisade textures and filaments (Fig. 4a–c) reveals that silicification of the original organic material has taken place. The presence of silicified ?mucus (Fig. 3c, arrow) and hollow central tubes (Fig. 4c, arrow) imply that microorganisms were active in several of these hot spring systems. In a detailed study of Ohaaki Pool, Jones et al. (1998) reported only rare preservation of open central tubes within masses of solid, granular, silicified microbial filaments identical to our Ohaaki Pool samples (Fig. 3b, c).

If oversaturation of silica in solution remains relatively low, then polymerisation does not occur (i.e. no spherical opal-A aggregates form) and silica can precipitate directly onto pre existing solid surfaces to produce a dense, vitreous silica deposit (Iler 1979; Weres and Apps 1982; Fournier 1985). This mechanism may explain certain microtextures observed in this investigation, for example, where thin smooth coatings of silica obscure primary opal-A aggregates (e.g. Fig. 3d). In addition, dense vitreous silica fills plant moulds (Fig. 3h). These dense vitreous layers can deposit quite early, depending on saturation state and flow rate of thermal fluids, or they may form later, to encrust opal-A spheres and organic matter with a layer of smooth, dense opal-A.

Bladed lepispheres (Fig. 4d) are common textural indicators of the next step in the ageing process: crystallisation to opal-CT (Flörke et al. 1975, 1991; Graetsch 1994). However, the origin of the fibrous amygdaloidal microcrystals associated with lepispheres in the Umukuri sinter (Fig. 4e) is not well understood, however, they may mark the onset of textural and mineralogic change toward quartz.

With the onset of quartz crystallisation at ~10,000 years, rosettes, drusy linings and elongate coarse crystals occupy cavities and fractures in older sinters (e.g. Fig. 4f–h). Quartz recrystallisation is typically a slow process (Knauth 1994).

Based on the data set for this study, the results reported herein suggest that the analysis of silica species and textural characterisation of silica sinter may offer a means of estimating the relatives ages of silica sinter deposits younger than 40,000 years, all other factors being equal. Effects other than time alone may need to be considered in interpreting a specific site. These include the presence of other materials, the temperature of initial deposition and the postdepositional history of the sinter, including any heating or burial it may have undergone (e.g. White et al. 1988).

The chemical composition of a silica sinter is not, in itself, a good guide to associated economic mineralisation, but presence of sinter alone may reveal the palaeohydrology of a former geothermal regime so that favourable prospecting sites can be located. In an area where chloride waters no longer discharge, Martin et al. (1999) have demonstrated how a pollen age of an in-situ sinter, can provide evidence of a worthwhile drilling target, given the longevity of geothermal fields. Where such immediate age information is lacking, the model offered here suggests how an ageing profile might be derived for an outcrop of sinter to help develop palaeohydrological information of an epithermal or geothermal prospect, prior to any drilling.

Acknowledgements This study was a part of the NZODA study award provided by the Ministry of Foreign Affairs and Trade (MFAT), New Zealand. Funds were contributed by the University of Auckland Research Committee. We thank Drs Kevin Brown and Ritchie Sims, and Svetlana Danilova, Yan Jing, Rod Martin and Karen Sannazzaro for assistance and/or fruitful discussions. Louise Cotterall and Andrea Afaro assisted with the figures. The manuscript was considerably strengthened by the helpful commentaries of Drs Graetsch and Renaut during refereeing. K.A. Rodgers is Research Associate, Australian Museum, Sydney, NSW 2000, Australia, and Kathleen A. Campbell is Research Associate in Geology, California Academy of Sciences, Golden Gate Park, San Francisco, CA 94118, USA.

References

Battey MH, Pring A (1997) Mineralogy for students. Longman, Edinburgh, 363 pp

Bignall G, Browne PRL (1994) Surface hydrothermal alteration and evolution of the Te Kopia thermal area, New Zealand. Geothermics 26: 645–658

Cady SL, Farmer JD (1996) Fossilization processes in siliceous thermal springs: trends in preservation along thermal gradients. In: Evolution of hydrothermal ecosystems on Earth (and Mars?). Ciba Foundation Symposium 202. Wiley, Chichester, pp 150–173

Cunneen R, Sillitoe RH (1989) Paleozoic hot spring sinter in the Drummond Basin, Queensland, Australia. Econ Geol 84: 135–142

Everett DH (1994) Basic principles of colloid science. Royal Society of Chemistry, Cambridge, 243 pp

Flörke OW, Jones JB, Segnit ER (1975) Opal-CT crystals. Neues Jahrb Mineral Monatsh H8: 369–377

Flörke OW, Graetsch H, Martin B, Röller K, Wirth R (1991) Nomenclature of micro- and non-crystalline silica minerals, based on structure and microstructure. Neues Jahrbh Mineral Abh 163: 19–42

Fournier RO (1985) The behaviour of silica in hydrothermal solutions. In: Geology and geochemistry of epithermal systems. Rev Econ Geol 2: 45–60

Fournier RO, Rowe JJ (1966) Estimation of underground temperatures from the silica content of water from hot springs and wet-steam wells. Am J Sci 264: 685–697

Graetsch H (1994) Structural characteristics of opaline and microcrystalline silica minerals. In: Heaney PJ, Prewitt CT, Gibbs GV (eds) Silica: physical behaviour, geochemistry and materials applications. Rev Mineral 29: 209–232

Graney JR (1987) Hasbrouck Mountain, Nevada, precious metal mineralization in a fossil hot springs environment. In: Johnson JL (ed) Bulk mineable precious metal deposits of the western United States. Guidebook for field trips. Geological Society of Nevada, Reno, Nevada, pp 120–125

Groves AW (1951) Silicate analysis, 2nd edn. Allen and Unwin, London, 336 pp

Henneberger RC, Browne PRL (1988) Hydrothermal alteration and evolution of the Ohakuri hydrothermal system, Taupo

Volcanic Zone, New Zealand. J Volcanol Geotherm Res 34: 211–231
Herdianita NR, Rodgers KA, Browne PRL (1999) Routine procedures for characterising modern and ancient silica sinter deposits. Geothermics (in press)
Iler RK (1979) The chemistry of silica. Wiley, New York, 866 pp
Jones B, Renaut RW (1996) Influence of thermophilic bacteria on calcite and silica precipitation in hot springs with water temperatures above 90 °C: evidence from Kenya and New Zealand. Can J Earth Sci 33: 72–83
Jones B, Renaut RW, Rosen MR (1997) Biogenicity of silica precipitation around geysers and hot-spring vents, North Island, New Zealand. J Sediment Res 67: 88–104
Jones B, Renaut RW, Rosen MR (1998) Microbial biofacies in hot-spring sinters: a model based on Ohaaki Pool, North Island, New Zealand. J Sediment Res 68: 413–434
Jones JB, Segnit ER (1971) The nature of opal I. Nomenclature and constituent phases. J Geol Soc Aust 18(1): 57–68
Kano K (1983) Ordering of opal-CT in diagenesis. Geochem J 17: 87–93
Kingma KJ, Hemley RJ (1994) Raman spectroscopic study of microcrystalline silica. Am Mineral 79: 269–273.
Knauth LP (1994) Petrogenesis of chert. In: Heaney PJ, Prewitt CT, Gibbs GV (eds) Silica: physical behaviour, geochemistry and materials applications. Rev Mineral 29: 233–256
Martin R, Mildenhall D, Browne PRL, Rodgers KA (1999) The age and significance of in-situ sinter at Te Kopia thermal area. Geothermics (in press)
Mizutani S (1977) Progressive ordering of cristobalitic silica in the early stage of diagenesis. Mineral Petrol 15: 129–140
Murata KL, Nakata K (1974) Cristobalitic stage in the diagenesis of diatomaceous shale. Science 184: 567–568
Murata KJ, Norman MB (1976) An index of crystallinity for quartz. Am J Sci 276: 1120–1130
Rimstidt JD, Cole DR (1983) Geothermal mineralization I: the mechanism of formation of the Beowawe, Nevada, siliceous sinter deposit. Am J Sci 283: 861–875
Sherlock RL, Tosdal RM, Lehrman NJ, Graney JR, Losh S, Jowett EC, Kesler SE (1995) Origin of the McLaughlin Mine sheeted complex: metal zoning, fluid inclusion and isotopic evidence. Econ Geol 90: 2156–2181
Smith DK (1997) Evaluation of the detectability and quantification of respirable crystalline silica by X-ray powder diffraction. Powder Diffraction 12(4): 200–227
Smith DK (1998) Opal, cristobalite, and tridymite: noncrystallinity versus crystallinity, nomenclature of the silica minerals and bibliography. Powder Diffraction 13(1): 2–19
Smykatz-Kloss W (1974) Differential thermal analysis: application and results in mineralogy. Springer, Berlin Heidelberg New York, 185 pp
Trewin NH (1994) Depositional environment and preservation of biota in the Lower Devonian hot-springs of Rhynie, Aberdeenshire, Scotland. Trans R Soc Edinburgh (Earth Sci) 84: 433–442
Walter MR, DesMarais D, Farmer JD, Hinman NW (1996) Lithofacies and biofacies of midPaleozoic thermal spring deposits in the Drummond Basin, Queensland, Australia. Palaios 11: 497–518
Walter MR, McLoughlin S, Drinnan AN, Farmer JD (1998) Palaeontology of Devonian thermal spring deposits, Drummond Basin, Australia. Alcheringa 22: 285–314
Weres O, Apps JA (1982) Prediction of chemical problems in the reinjection of geothermal brines. Geol Soc Am Spec Pap 189: 407–426
White DE, Hutchinson RA, Keith TEC (1988) The geology and remarkable thermal activity of Norris Geyser Basin, Yellowstone National Park, Wyoming. US Geol Surv Prof Pap 1456: 1–84
White DE, Thompson GA, Sandberg CH (1964) Rocks, structure, and geologic history of Steamboat Springs Thermal Area, Washoe County, Nevada. US Geol Surv Prof Pap 458-B, B1–B63
White IG, Grimshaw RW (1970) The determination of crystalline quartz by differential thermal analysis: a modification to technique. Trans J Brit Ceram Soc 69: 175–176
White NC, Wood DG, Lee MC (1989) Epithermal sinters of Paleozoic age in north Queensland, Australia. Geology 17: 718–722